

Quantification of the memory effect of steady-state currents from interaction-induced transport in quantum systems

Chen-Yen Lai* and Chih-Chun Chien

School of Natural Sciences, University of California, Merced, Merced, California 95343, USA

(Received 1 June 2017; published 22 September 2017)

Dynamics of a system in general depends on its initial state and how the system is driven, but in many-body systems the memory is usually averaged out during evolution. Here, interacting quantum systems without external relaxations are shown to retain long-time memory effects in steady states. To identify memory effects, we first show quasi-steady-state currents form in finite, isolated Bose- and Fermi-Hubbard models driven by interaction imbalance and they become steady-state currents in the thermodynamic limit. By comparing the steady-state currents from different initial states or ramping rates of the imbalance, long-time memory effects can be quantified. While the memory effects of initial states are more ubiquitous, the memory effects of switching protocols are mostly visible in interaction-induced transport in lattices. Our simulations suggest that the systems enter a regime governed by a generalized Fick's law and memory effects lead to initial-state-dependent diffusion coefficients. We also identify conditions for enhancing memory effects and discuss possible experimental implications.

DOI: [10.1103/PhysRevA.96.033628](https://doi.org/10.1103/PhysRevA.96.033628)

I. INTRODUCTION

Although dynamic processes generally depend on the initial conditions and evolution protocols, many-body systems tend to average out, in the long-time limit, memory of initial information. Take metals as an example; the fast relaxation time quickly brings the electrons to a new equilibrium or steady state after a perturbation [1–3]. Therefore, systems exhibiting long-time or persistent memory effects, for instance, magnetic hysteresis [4], shape-memory materials [5], and memory-effect elements and circuitries [6,7], are considered interesting. Moreover, artificial spin ice driven by a cyclic magnetic field shows memory effects of reproducible microstates [8]. In a partial symmetry-breaking Hamiltonian, the symmetry memory and symmetry gap show quantum memory effects of initial states below a critical value [9]. Other examples of memory effects in quantum systems include ferroelectric semiconductor [10,11] and magnetic [12,13] materials.

Moreover, the concept of memory effects is related to the existence of fundamental limits in many-body quantum systems on the relaxation of current [14] and development of thermal equilibrium [15]. For example, systems exhibiting many-body localization [16–19] can fail to thermalize, show ergodicity breaking [20], and retain local information about the initial condition at long times [21]. The out-of-time-order correlation functions [22–24] provide another useful measure to diagnose the sensitivity of time-evolving quantities to the initial condition and offer a tool to investigate fast scrambling of information [25]. Cold-atom systems, with their broadly tunable parameters, are suitable for elucidating key mechanisms behind quantum transport [26]. Memory effects, in the form of hysteresis, have been explored in cold-atom experiments of atomic superfluids [27] and a theoretical proposal of spin-orbit-coupled Fermi gases [28]. Energy dissipation was included by vortex generation or external reservoirs in those hysteresis studies. In addition, memory effects of

open quantum systems coupled to classical and quantum environments have also been intensely studied [29,30]. Here we investigate memory effects in isolated quantum systems without explicit relaxations.

In the absence of interactions, dynamical variables of quantum systems, such as the mass current, are usually found not to exhibit memory effects in steady states [31–34]. To identify long-time memory effects, the density of a tunable bound state may provide clues when the system is at steady state [31]. A flat band coming from localized states after a continuous transformation of the underlying lattice geometry also reveals memory effects of the transformation rate in the steady-state density distribution [35]. Moreover, memory effects of entanglement and correlation can arise from topological edge states as boundary conditions [36–38] or as parameters [39] are changed. In addition, quench dynamics of integrable systems can exhibit memory effects, where a steady state emerges and depends strongly on the initial condition [40–42]. In contrast, interacting quantum systems can exhibit memory effects directly in the steady-state current as illustrated in Luttinger liquids [43], where currents driven by different quench procedures reach different steady-state values.

Here we quantify long-time memory effects in the steady-state current of isolated interacting quantum systems, including both fermionic and bosonic gases. Since transport usually singles out a particular direction, we consider one-dimensional (1D) lattice systems where particle hopping due to tunneling slows down the motion. To focus on intrinsic effects, the current can be induced, for example, internally by switching on a spatial interaction imbalance, so there is no need for an external source and sink. In a finite system, the boundary reflects the wave function and leads to a revival time which linearly scales with the system size. However, a quasi-steady-state current (QSSC) emerges before the revival time and allows us to quantify memory effects by comparing the steady-state values from different driving protocols. As the system size L scales toward the thermodynamic limit, the revival time scales toward infinity ($L \rightarrow \infty$ and then $t \rightarrow \infty$). The QSSCs then become genuine steady-state currents and memory effects revealed by

*Current address: Theoretical Division, Los Alamos National Laboratory, Los Alamos, New Mexico 87545, USA; chengyanlai@gmail.com

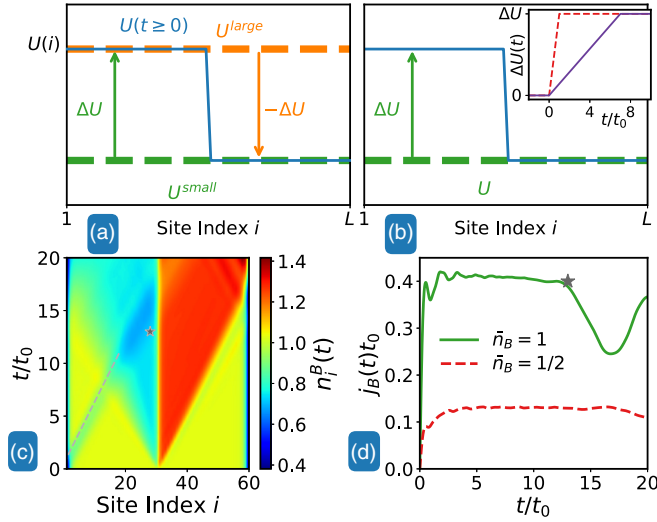


FIG. 1. Interaction-induced transport for probing (a) memory effects of initial states and (b) memory effects of switching protocols. (a) Two systems initially with different uniform interactions U^{small} (dashed green) and U^{large} (dashed orange) are quenched to the same interaction profile (solid blue). (b) Systems with the same initial interaction (dashed green) experience the same interaction imbalance (solid blue) switched on at different time scales. Inset: Linear switching protocols with different ramping times ($t_r = t_0, 7t_0$). (c, d) Interaction-induced transport in the BHM. (c) Particle density contour plot with $L = 60$ sites, $\bar{n}_B = 1$, $U = J$, and $\Delta U = J$ on the left half of the lattice. The dashed line in (c) indicates the propagation of the low-density region from the left edge and the red star marks the time at which the density distortion affects the QSSC; as one can see the QSSC decreases at the gray star in (d). The red (light-blue) regime on the right (left) half of the system indicates the formation of density plateaus. (d) Current flowing through the interface of the interaction imbalance with different fillings and $U = \Delta U = J$. The stars in (c) and (d) indicate the same time ($t = 13t_0$).

the different values of currents persist in the long-time limit. In isolated systems discussed here, the transient regime before the system enters the quasi-steady state does not scale with the system size. Therefore, the steady state in the thermodynamic limit is similar to the quasi-steady state of a large but finite system and memory effects can be identified by comparing the steady-state currents.

Two types of memory effects are analyzed here, one from different initial states and the other from different protocols of inducing transport. To distinguish the two memory effects, we use different ways to turn on the spatial interaction or potential imbalance. For the first type of memory effects, we consider systems with different initial ground states but quenched to the same final interaction or potential profile as illustrated in Fig. 1(a). For the second type, the same imbalance is switched on linearly with different time scales (t_r) as shown in Fig. 1(b). Here we present the results of interaction-induced transport in lattices and discuss continuous models and potential-driven transport. While memory effects of initial states are visible in all of these settings, memory effects of switching protocols are mostly visible only in interaction-induced transport in lattices.

The paper is organized as follows. Section II introduces the models and simulation methods, and then we present

the results from interaction-induced transport. Section III discusses memory effects of initial states and memory effects of switching protocols. The continuous model is discussed in Sec. IV and serves as a comparison. Section V presents a connection between Fick's law and our studies and the diffusion coefficients extracted from the relation. Section VI is devoted to potential-induced transport and its memory effects. In Sec. VII we discuss experimental implications of cold atoms, possible implementations, and how memory effects of steady-state currents may be measured. A conclusion is given in Sec. VIII.

II. INTERACTION-INDUCED TRANSPORT

A mass current can be induced by imposing an interaction imbalance as illustrated in Figs. 1(a) and 1(b). We consider two lattice models: The Hamiltonian of the Bose-Hubbard model (BHM) is given by

$$\mathcal{H}_{\text{BHM}} = -J \sum_{\langle i,j \rangle} (b_i^\dagger b_j + \text{H.c.}) + \sum_i \frac{U(i,t)}{2} n_i (n_i - 1). \quad (1)$$

Here b_i^\dagger (b_i) is the boson creation (annihilation) operator at lattice site i , $n_i = b_i^\dagger b_i$ is the boson number operator at site i , and $\langle i,j \rangle$ represents nearest neighbors. We set $\hbar = 1$ and the time unit is $t_0 = \hbar/J$. The Fermi-Hubbard model (FHM) has the Hamiltonian

$$\mathcal{H}_{\text{FHM}} = -J \sum_{\langle i,j \rangle, \sigma} (c_{i,\sigma}^\dagger c_{j,\sigma} + \text{H.c.}) + \sum_i U(i,t) n_{i,\uparrow} n_{i,\downarrow}. \quad (2)$$

The two components of fermions are usually two different hyperfine states of the same species of atoms and we use $\sigma = \uparrow, \downarrow$ to label them. Here $c_{i,\sigma}^\dagger$ ($c_{i,\sigma}$) is the fermion creation (annihilation) operator at lattice site i with spin σ , and $n_{i,\sigma} = c_{i,\sigma}^\dagger c_{i,\sigma}$ is the fermion number operator at site i with spin σ . The filling of the BHM is $\bar{n}_B = \sum_i n_i / L$. We consider \bar{n}_B up to 1 for a system with $L = 60$ sites and monitor the current at the interaction-imbalance interface, so $j_B = 2J \text{Im} \langle b_{L/2+1}^\dagger b_{L/2} \rangle$. As for the FHM, we consider the spin-balanced case where $N_\uparrow = \sum_i n_{i,\sigma} = N_\downarrow$ with filling $\bar{n}_F = N_\sigma / L$ up to 1/2, and the current is the total current $j_F = 2J \text{Im} \langle \sum_\sigma c_{L/2+1,\sigma}^\dagger c_{L/2,\sigma} \rangle$.

Initially, an uniform interaction is applied throughout the system and the ground state can be obtained by the density matrix renormalization group [44–49]. Then a spatial interaction imbalance is imposed on half of the system, as illustrated in Fig. 1. A positive (negative) interaction imbalance ΔU is applied to the left (right) half of the system so the final Hamiltonian always has a higher interaction energy in the left half of the system. The dynamics can be simulated with the time-dependent density matrix renormalization group [47,49–52] using the second-order Suzuki-Trotter formula with time step $\delta t = 0.005t_0$. During the simulation, the maximum bond dimension is kept up to $\chi = 1000$ states and we are able to maintain the maximal truncation error below 10^{-7} . Most of the simulations are performed with system size $L = 60$. By comparing the results from different values of L , we have ensured that $L = 60$ is large enough for the same result to be qualitatively observed in the thermodynamic limit.

A typical example of the interaction-induced dynamics is shown in Figs. 1(c) and 1(d). Right after the interaction

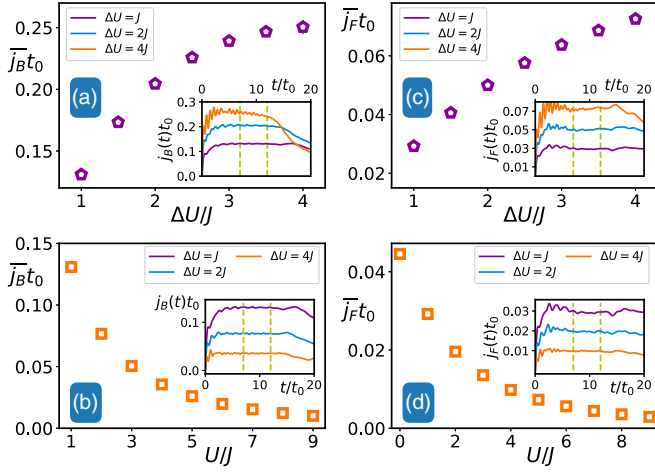


FIG. 2. QSSCs in the BHM with $\bar{n}_B = 1/2$ and FHM with $\bar{n}_F = 1/6$. Insets: The evolution of mass current, where the plateaus indicate the QSSC, and dashed lines indicate the time window in which the averages are taken. (a) BHM and (c) FHM with the same uniform initial interaction $U = J$ and different interaction imbalances. (b) BHM and (d) FHM with different uniform initial interactions and the same interaction imbalance, $\Delta U = J$. A stronger initial interaction suppresses the QSSC value. Error bars are the standard deviation from the time average and they are within the symbol size if not shown.

imbalance is applied, the system passes through a transient regime ($t < 4t_0$), and then the density in the left and right halves starts to develop plateaus ($t = 10t_0$) as show in Figs. 1(c) and 9(a). The existence of the density plateaus is important for the QSSC to emerge. As the plateaus develop, the density gradient around the interface of the interaction imbalance will be constant when the QSSC is observable. This indicates that the system may be describable by coarse-grained kinetic equations [53,54] connecting the density and current. We emphasize that the transport is induced by changing the coupling strength in the Hamiltonian only, and there is no external exchange of energy or particle because the system is isolated.

The results of interaction-induced transport are summarized in Figs. 2 and 3. QSSCs can be observed as the plateaus in the insets in Figs. 2 and 3, and they will become genuine steady states in the thermodynamic limit. While the QSSC can be observed in interacting bosonic and fermionic systems, its existence in noninteracting systems is less trivial. Homogeneous noninteracting bosons do not support QSSCs [55], and we observe no QSSC if half of the bosonic system is noninteracting during the dynamics, which is discussed later in this section. For fermions, QSSCs already exist in the absence of interactions [32,56]. If $\bar{n}_F < 1/2$ or $\bar{n}_B < 1$, a larger interaction imbalance results in a larger QSSC under the same initial condition. On the other hand, the QSSC value gets smaller but never reaches 0 as the initial interaction is stronger while the interaction imbalance is fixed, as shown in Figs. 2(b) and 2(d).

A. Additional features at higher filling

At or above $\bar{n}_F = 1/2$ or $\bar{n}_B = 1$, strong interactions lead to additional phenomena. For example, negative differential conductance (NDC), where the current decreases as the driving

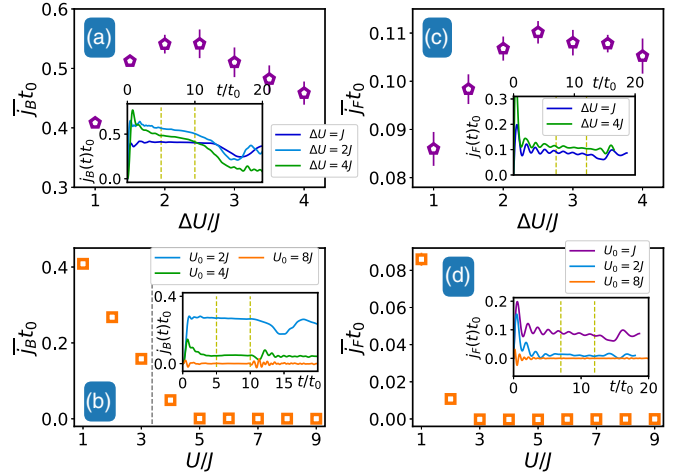


FIG. 3. Interaction-induced transport by a sudden interaction imbalance of (a, b) the BHM with $\bar{n}_B = 1$ and (c, d) the FHM with $\bar{n}_F = 1/2$. The system size is $L = 60$ sites. Under a constant initial interaction $U = J$, the QSSCs as a function of the interaction imbalance are shown in (a) for the BHM and (c) for the FHM. By quenching the systems with the same $\Delta U = J$ in the left half, the QSSCs decrease with the initial interaction as shown in (b) for the BHM and (d) for the FHM. The dashed line in (b) indicates the critical interaction of the 1D superfluid–Mott insulator transition. Insets: Current versus time for selected values labeled on the graph. Dashed lines indicate the time window in which the average is taken.

force increases, has been discussed in fermions [32] and observed in bosons [57]. In isolated systems, energy conservation can lead to dynamically insulating phases [32,58]. Moreover, the Mott insulating phase at $\bar{n}_B = 1$ or $\bar{n}_F = 1/2$ with moderate initial interactions can be destroyed by a strong potential bias [59–61] or interaction imbalance.

1. Bose-Hubbard model at unity filling

The main results of the BHM at unity filling are presented in Figs. 3(a) and 3(b), where the symbols show the time average of QSSCs and the statistical standard deviation within a selected time window is indicated by the error bar. As a larger interaction imbalance shrinks the duration of QSSCs due to the boundary effect, we did not observe the NDC when filling was lower than 1 within the parameter range we searched. For BHM at unity filling in the thermodynamic limit, the Mott-superfluid transition occurs at the critical interaction $U_c \approx 3.37J$ in one dimension [62,63].

In Fig. 3(a), the system is initially a superfluid with $U = J$ and the QSSCs do not increase monotonically with ΔU , which is different from the behavior at low fillings. The QSSCs increase with the interaction imbalance when ΔU is small, but the dependence changes once the interaction imbalance is above $2.5J$, beyond which the response (current) starts to decrease as the driving (interaction imbalance) increases. Similar phenomena are also discovered in theory [58,64] and cold-atom experiments [57,64]. For filling larger than unity, the systems are expected to suffer NDC as well when the interaction imbalance increases. The origin of NDC is because the interaction imbalance causes an energy difference between the two sides of the system. Since the isolated system respects energy

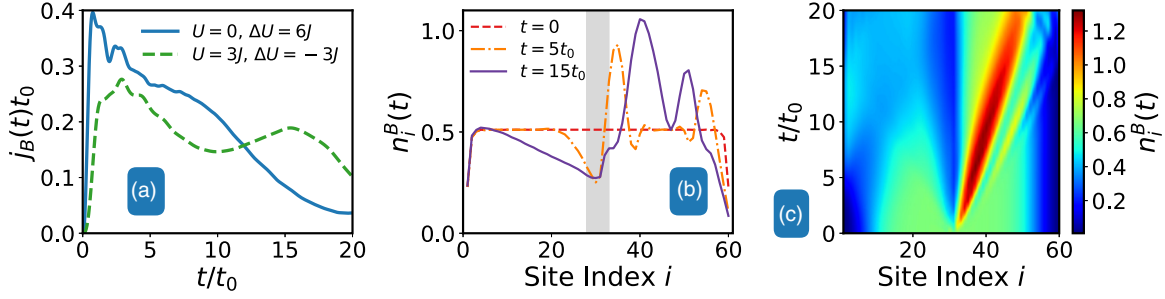


FIG. 4. No QSSC can be observed if part of a bosonic system is noninteracting. (a) Currents through the middle of a lattice with $L=60$ sites and $\bar{n}_B=1/2$ versus time for two cases: initially noninteracting bosons experiencing an interaction imbalance (solid blue line) and initially interacting bosons with part of the system quenched to noninteracting bosons (dashed green line). (b) Particle density profiles at selected times for a system with an initial interaction $U=3J$ and an imbalance $\Delta U=-3J$ applied to the right half. There are no steady structures in the central (shaded) region compared to Fig. 9(a). (c) Evolution of the particle density for $U=0$ and $\Delta U=6J$ in the left half.

conservation, changes in the interaction energy have to be compensated for by the kinetic energy. As the interaction difference gets larger, it is harder for the two sides to exchange particles in an energy-conserved fashion. Eventually, if the energy difference between the two parts of the system greatly exceeds the band width, a dynamically nonconducting state emerges because it is not possible to exchange particles without violating energy conservation in an isolated system. The boundary effect limits our simulations with strong interaction imbalance as shown in the inset in Fig. 3, where the error bars become larger due to the distortion of the wave function from the edge.

If the interaction energy is within the range of the bandwidth, the system does not become dynamically insulating if the initial state is in the superfluid regime. However, the QSSC becomes smaller as the initial interaction increases with the same quenched interaction imbalance. A finite QSSC is still observable for a system with initial interaction $U=4J > U_c$ in the Mott insulator regime and experiencing an interaction imbalance $\Delta U=J$ on the left as shown in Fig. 3(b). This indicates a dynamic breakdown of the Mott insulating state by an interaction imbalance. The reason for the breakdown is that at the interface of the interaction imbalance it is preferable to have a doublon-holon pair (with a hole on the stronger-interaction side and two bosons at one site on the weaker-interaction side) and lower the local interaction energy. Creating this pair of excitations requires more energy as the initial interaction increases, and eventually a fixed ΔU is no longer sufficient to produce the pair. Thus, the QSSC vanishes in the strong-interaction regime as shown in Fig. 3(b). The destruction of the Mott insulating state has also been addressed by applying a strong potential imbalance to a Mott insulator [61,65] and the destruction can be understood by a many-body Schwinger-Landau-Zener mechanism [59,60].

2. Fermi-Hubbard model at half-filling

For the FHM with a filling smaller than half, the transport behavior is qualitatively the same as that of the BHM discussed in Sec. II, except QSSCs exist in fermions even in the absence of interactions [32]. The 1D FHM has a charge gap for any nonzero interaction $U > 0$ at half-filling in the thermodynamic limit according to the exact solution [66]. Thus, both the NDC and the dynamically insulating state are expected to happen in the FHM at half-filling, and indeed they are shown

in Figs. 3(c) and 3(d). Similarly to the BHM, with small initial interactions like $U=J$ and $U=2J$, it is possible to break the Mott insulating state by a strong interaction imbalance through the mechanism of a doublon and holon pair, similarly to the BHM case. When the initial interaction or the energy imbalance greatly exceeds the bandwidth, energy conservation prevents exchange of particles with a large energy difference and the system will remain an insulator.

B. Absence of QSSCs in noninteracting bosons

For bosonic systems, we found that QSSCs can only exist when the interactions in both halves are finite. To check the absence of QSSCs if part of the system is noninteracting, we consider two cases here: One starts from a noninteracting system and then the left half is quenched to a finite interaction. The second is initially a uniform, interacting system and the interaction in the right half is turned off. The results are shown in Fig. 4(a), and there is no QSSC in either case. The reason that noninteracting Bose gases cannot support QSSC is the infinite compressibility, which allows bosons to pile up without limit if there is no interaction energy. According to the kinetic equation approach [53,54] shown in Eq. (5), the QSSCs depend on a constant density gradient at the interface. If half of the system is noninteracting, the bosons will keep stacking up and never reach a plateau as shown in Fig. 4(b). This can also be observed by comparing Figs. 4(c) and 1(c).

III. MEMORY EFFECTS

By comparing the QSSCs induced by different protocols, we can quantify memory effects at steady state. Previous studies of interaction-induced transport [32] using a mean-field approximation failed to observe memory effects because multiparticle correlations were ignored, but here we found two main causes of memory effects: the initial state and the protocol for switching on the interaction imbalance.

A. Memory effects of initial states

To analyze the memory effects of initial states, we introduce different interaction imbalances so that different initial configurations are suddenly changed to the same final configuration, and the system evolves accordingly. As illustrated in

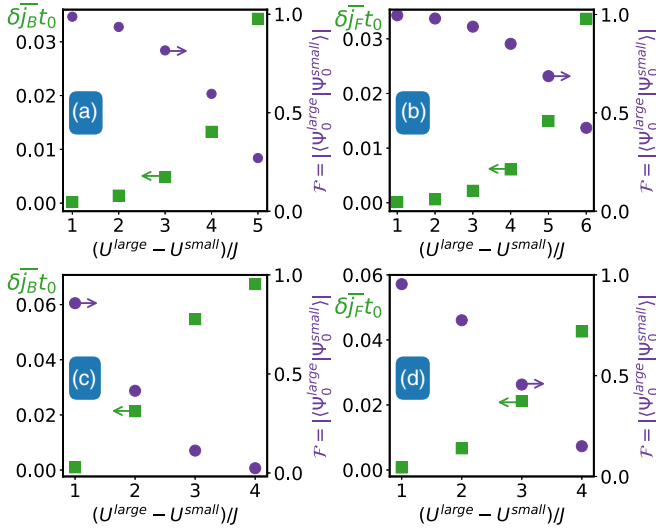


FIG. 5. Memory effects of initial states for the BHM with (a) $\bar{n}_B = 1/2$ and (c) $\bar{n}_B = 1$ and for the FHM with (b) $\bar{n}_F = 1/6$ and (d) $\bar{n}_F = 1/2$. Squares correspond to the difference in the steady-state currents from two initial interactions $U^{\text{large}} = 6J$ and U^{small} , which can be inferred from the $(U^{\text{large}} - U^{\text{small}})/J$ values, quenched to the same final interaction profile. Circles show the fidelity \mathcal{F} between the two initial ground states.

Fig. 1(a), one can consider two initial configurations, one with $U(i) = U^{\text{small}}$ and one with $U(i) = U^{\text{large}}, \forall i$. The difference between the two initial ground states can be quantified by the fidelity $\mathcal{F} = |\langle \Psi_0^{\text{large}} | \Psi_0^{\text{small}} \rangle|$. Then sudden quenches at $t=0$ are applied to the two systems so that $\Delta U = U^{\text{large}} - U^{\text{small}} > 0$ is applied to the left half of the first system, and $-\Delta U$ is applied to the right half of the second system. After the quenches, both systems have the same interaction profile, with U^{large} (U^{small}) in the left (right) half. Comparing the QSSCs of the two systems then reveals the memory effect from initial states.

The difference in steady-state values of the currents and the fidelities of the initial states are shown in Fig. 5(a) for bosons with $\bar{n}_B = 1/2$ and in Fig. 5(b) for fermions with $\bar{n}_F = 1/6$. Here, the current is averaged over a time period within the steady-state regime, $\overline{j_{B(F)}} = \sum_{t=t_i}^{t_f} \Delta t j_{B(F)}(t) / (t_f - t_i)$ with $\Delta t = 0.02t_0$, and the difference in averaged currents between the two initial states are $\delta \overline{j_{B(F)}} = |\overline{j_{B(F)}^{\text{large}}} - \overline{j_{B(F)}^{\text{small}}}|$. As one can see, even though the final Hamiltonians are identical, the steady-state currents do not necessarily agree. A larger difference in the averaged currents indicates stronger memory effects. In the same plot, the fidelity between the two initial states shows that the steady-state memory effects are stronger as the two initial states have less overlap. Interestingly, there is no qualitative difference between the bosonic and the fermionic results. The correlations from interactions, which are missing in mean-field theory [32], are important for correctly describing memory effects.

The BHM with $\bar{n}_B = 1$ is a Mott insulator for the system initially with $U^{\text{large}} = 6J$ and the one initially with $U^{\text{small}} = 5J$, so the QSSC induced by $\Delta U = J$ is 0 and no memory effects can be identified in Fig. 5(c). When using a smaller U^{small} (a stronger ΔU) as the initial condition, the fidelity between the two initial wave functions decreases, and memory effects

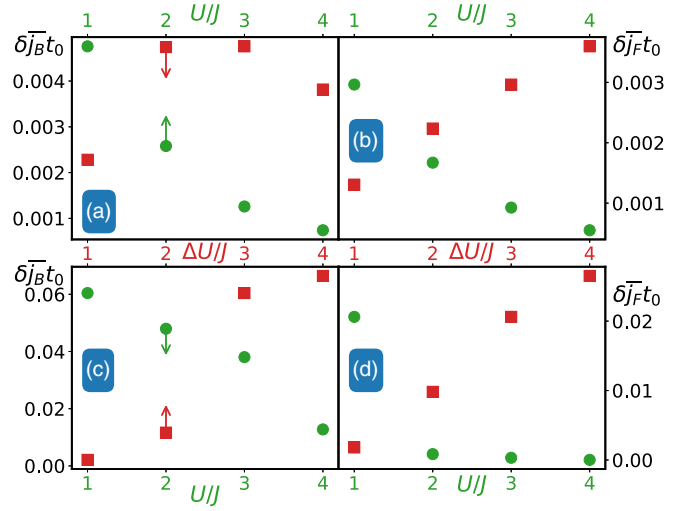


FIG. 6. Memory effects of switching protocols for the BHM with (a) $\bar{n}_B = 1/2$ and (c) $\bar{n}_B = 1$ and for the FHM with (b) $\bar{n}_F = 1/6$ and (d) $\bar{n}_F = 1/2$. Memory effects of switching protocols are probed with different finite ramping times $t_r = t_0$ and $7t_0$ for varying interaction imbalances but a fixed initial interaction, $U = J$ (red squares), and for different initial interactions but the same interaction imbalance, $\Delta U = 3J$ (green circles). A larger difference in the averaged steady-state currents indicates stronger memory effects. Starting with $U = J$, memory effects become stronger as the interaction imbalance increases. Memory effects are suppressed when the initial interaction is strong. For $t_r = t_0$ ($7t_0$), the averages are taken between $5t_0$ and $10t_0$ ($10t_0$ and $15t_0$).

start to emerge. After comparing different fillings with the same parameter settings, we found that bosons at unity filling exhibit stronger memory effects than bosons at low fillings. Similar phenomena are also observed in the FHM as shown in Fig. 5(d).

B. Memory effects of switching protocols

The second kind of memory effects arises from different switching protocols, and here we focus on its dependence on the ramping time when the interaction imbalance is switched on linearly in time. Taking two systems with the same initial and final configurations but with different ramping time scales as illustrated in Fig. 1(b) and its inset, the memory effects from different ramping time scales can then be identified from the different QSSCs. The results are shown in Fig. 6, where we chose two time scales $t_r = t_0$ and $7t_0$ and compare the steady-state values. The figure shows the difference in average currents between two time scales, $\delta \overline{j_{B(F)}} = |\overline{j_{B(F)}^{7t_0}} - \overline{j_{B(F)}^{t_0}}|$. We have checked other values of t_r between $5t_0$ and $7t_0$, and there is no qualitative difference. We also found that, in general, fermions exhibit stronger memory effects. On the other hand, if the ramping of interaction imbalance becomes slower and eventually reaches the adiabatic limit, i.e., $t_r \rightarrow \infty$, there will be no finite QSSCs, as the system remains in the equilibrium state during time evolution.

Figure 6 offers clues on enhancing the memory effects of switching protocols. With the initial interaction fixed, a larger interaction imbalance tends to cause stronger memory

effects regardless of the filling. For a finite system, a stronger interaction imbalance can lead to stronger boundary effects and limit the time a QSSC can be maintained. Thus, the memory effects of switching protocols are more visible in interaction-induced transport with a larger interaction imbalance and smaller initial interaction.

For the BHM at unity filling and the FHM at half-filling, the general conclusion still holds, as memory effects of steady-state currents are amplified when applying a stronger interaction imbalance with a weaker initial interaction. However, both the BHM and the FHM will suffer the dynamically insulating state in the large interaction-imbalance regime, and there we cannot find QSSCs or resolve memory effects in our simulations. In the regimes where QSSCs can be sustained, our results show that stronger memory effects can occur when the BHM is at unity filling and the FHM is at half-filling as shown in Figs. 6(c) and 6(d).

While memory effects of switching protocols are observable in interaction-induced transport in both the BHM and the FHM, they are more fragile in other settings, partly because short-time correlations are usually averaged out. The system enters the regime described by kinetic equations and is insensitive to its transient behavior [53,54,67,68].

IV. CONTINUUM MODEL

To verify the ubiquity of memory effects, we also consider weakly interacting bosons in the continuum. The zero-temperature Bose-Einstein condensate and its dynamics may be studied by the mean-field Gross-Pitaevskii equation (GPE) [69,70]. It can be generalized to describe time-dependent systems [71–73] and has been previously implemented in modeling coherent transport [74,75]. In one dimension, the time-dependent GPE can be written as

$$\left[-\frac{\hbar^2}{2m} \frac{d^2}{dx^2} + V_{\text{ext}}(x) + \tilde{U}(x,t)N_b |\Phi|^2 \right] \Phi = i\hbar \frac{\partial}{\partial t} \Phi, \quad (3)$$

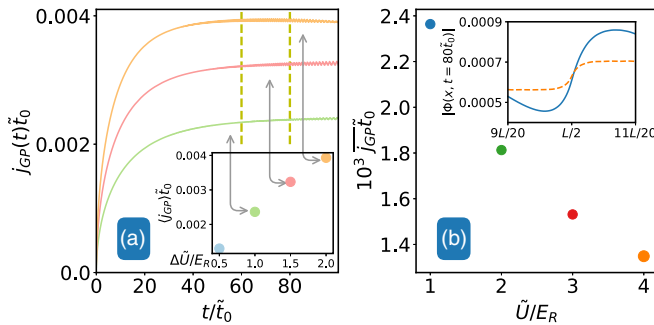


FIG. 7. Dynamics of the GPE for $N_b=10$ bosons under (a) a constant initial interaction $\tilde{U}=E_R$ and (b) a constant interaction imbalance $\Delta\tilde{U}=E_R$. The results show decreasing QSSCs with increasing initial interaction or decreasing interaction imbalance. Statistical errors are within the symbol size and dashed lines indicate the regime where the average is taken. Inset in (a): Averaged currents for different interaction imbalances. Inset in (b): Amplitudes of the condensate wave function near the center of the system (shaded region) at time $t=80\tilde{t}_0$ for two initial interactions, $\tilde{U}=E_R$ (dashed red line) and $\tilde{U}=4E_R$ (solid blue line).

where $\Phi(r,t)$ is the condensate wave function, m is the mass of the bosonic atom, and N_b is the number of bosons. The coupling constant $\tilde{U}=4\pi\hbar^2 a_s/m$ is determined by the two-body s -wave scattering length a_s . In our simulation, the external potential $V_{\text{ext}}(x)$ corresponds to a box potential which confines the atoms. Here we solve the GPE with algorithms involving real- and imaginary-time propagation based on a split-step Crank-Nicolson method [71,76] and follow Ref. [77] to normalize the wave function with $\int dx |\Phi(x)|^2 = 1$.

A. Quasi-steady-state current

The initial state is the ground state of a system with size l and a uniform interaction \tilde{U} . The energy unit is the recoil energy $E_R=\pi^2\hbar^2/2ml^2$ and the time unit is $\tilde{t}_0=\hbar/E_R$. At time $t=0$, the interaction imbalance is suddenly imposed with $\Delta\tilde{U}$ in the left half of the system, and we monitor the current flowing through the middle, which can be calculated by

$$j_{\text{GP}}(t) = \frac{d}{dt} \int_0^{L/2} dx N_b |\Phi(x,t)|^2. \quad (4)$$

In Fig. 7(a), the current reaches a plateau, indicating the existence of a QSSC. The duration of the QSSC scales as the system size increases, and the steady-state value allows us to quantify memory effects unambiguously. We calculate the averaged current $\bar{j}_{\text{GP}} = \sum_{t=t_i}^{t_f} \Delta t j_{\text{GP}}(t) / (t_f - t_i)$ in a time window (t_i, t_f) where the QSSC lasts. Under the same initial interaction, the QSSC increases as a larger interaction imbalance is applied, as shown in the inset in Fig. 7(a). Macroscopically, the current is driven by the pressure difference between the two sides of the interaction imbalance. On the other hand, the QSSC decreases as the initial interaction is stronger, as shown in Fig. 7(b). This is because a larger interaction presents

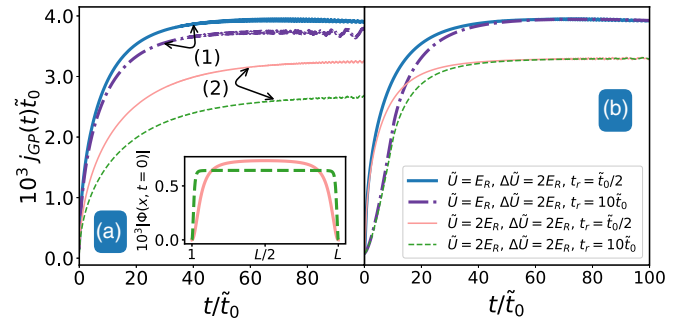


FIG. 8. Memory effects of weakly interacting Bose gases described by the GPE. (a) Two examples under different initial conditions. Both cases reach the same final interaction configuration with \tilde{U}^{large} in the left half and \tilde{U}^{small} in the right half. In case (1), $\tilde{U}^{\text{large}}=3E_R$ (dashed-dotted purple line) and $\tilde{U}^{\text{small}}=E_R$ (thick solid blue line) are compared. In case (2), $\tilde{U}^{\text{large}}=1.5E_R$ (dashed green line) and $\tilde{U}^{\text{small}}=0.5E_R$ (thin solid red line) are compared. The two examples show that the QSSCs depend on the initial conditions. Inset: Initial profiles of the condensate wave functions for $\tilde{U}=0.5E_R$ (solid red line) and $\tilde{U}=1.5E_R$ (dashed green line), respectively. (b) Ramping of an interaction imbalance with finite time scales $t_r = \tilde{t}_0/2, 10\tilde{t}_0$ for systems with $N_b=10$ bosons for the two cases $\tilde{U}=\Delta\tilde{U}/2=E_R$ (top two lines) and $\tilde{U}=\Delta\tilde{U}=2E_R$ (bottom two lines). QSSC values from different ramping times cannot be distinguished in either case.

a larger initial pressure and applying the same interaction imbalance triggers a smaller percentage change in the pressure. While the transport properties of the GPE are similar to that of the BHM, the GPE does not exhibit the superfluid–Mott insulator transition.

B. Memory effects of the continuum model

The memory effects of initial states can be observed in the two examples of the GPE shown in Fig. 8(a). We note that memory effects of initial states are more prominent in the dilute limit (with a small N_b), as the two initial interactions provide the more distinct density profiles shown in the inset in Fig. 8(a). If the density is high (with a large N_b) and the two interactions are too strong in the beginning, the resulting initial states can be very similar and the memory effects will be difficult to resolve. On the other hand, in Fig. 8 (b) we show two examples which start with the same initial condition and reach the same final configuration but with different ramping times t_r . In both examples, the steady-state values are the same and there is no observable memory effect.

For the memory effects of switching schemes to survive, the short-time correlations should not be averaged out completely. This requires the Green’s function to depend sensitively on short-time changes. However, this is probably not the case in the continuum limit because the minimum difference in the intrinsic time scale is determined by $\Delta\tilde{t}_{\min} \sim \hbar/\Delta E_{\max}$, where E_{\max} may be identified as the width of the energy spectrum. Since E_{\max} has no upper bound in the continuum model but is bounded by the bandwidth in lattice models, the Green’s function always reduces to the “short-memory” approximation in the continuum model because one t_0 corresponds to many $\Delta\tilde{t}_{\min}$ as the system evolves. As a consequence, short-time correlations may survive and cause memory effects of switching protocols in lattice models, but they are mostly averaged out in the continuum.

V. FICK’S LAW AND GENERALIZED DIFFUSION COEFFICIENT

In the absence of interactions, the transport is ballistic and one may use the Landauer theory [54,78] to evaluate the current if the system is connected to two particle reservoirs. On the other hand, in interacting systems the numerous energy levels may serve as a reservoir for the system itself [53]. After averaging out the short-term correlations, one may obtain a quantum kinetic equation for the density rather than the wave function [53,67]. In one dimension, it has a form similar to that of Fick’s law:

$$j(x,t) = -D(x,t)\frac{\partial}{\partial x}n(x,t). \quad (5)$$

However, the diffusion coefficient $D(x,t)$ can be a function of the time and position and may be obtained from the space-time integral of the real-time Green’s function $G(x-x';t-t')$. For instance, $D(x,t) = \frac{\int_{-\infty}^t w(t')dt' \int G(x-x';t-t')dx}{w(t) \int G(x-x';t-t')dx}$, where $w(t)$ describes how the driving is introduced. The classical diffusion limit may be obtained by using a slowly varying function in the interval $(-\infty,t)$ for $w(t)$ with the additional assumptions of linearity, the long-wavelength restriction characteristic of

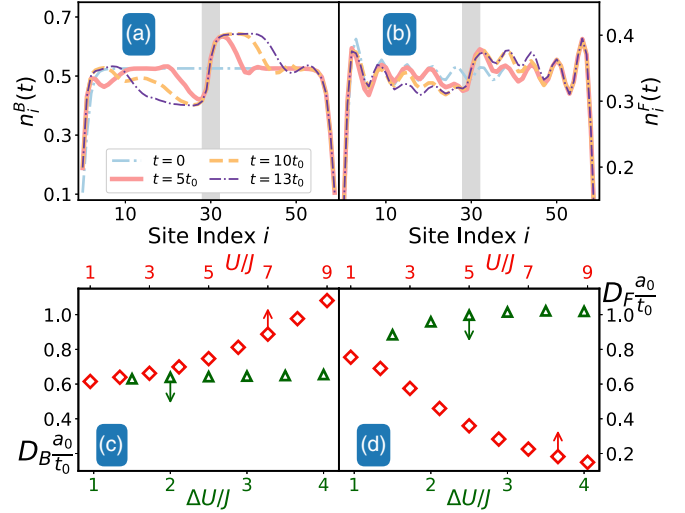


FIG. 9. Evolution of density profiles and diffusion coefficients of (a, c) the BHM with filling $\bar{n}_B = 1/2$ and (b, d) the FHM with $\bar{n}_F = 1/6$ on a 60-site lattice. A constant density gradient appears near the interface of the interaction imbalance (shaded region) when the steady-state current lasts. (a) and (b) start with $U = J$ and undergo an interaction imbalance quench $\Delta U = J$ on the right half. (c) and (d) fix $\Delta U = J$ (or $U = J$) and vary U (or ΔU). Here a_0 is the lattice constant.

simple fluids, and the time interval $t - t'$ being of the order of the mean free time.

At this point, the equation is still complicated, so it is common to use the short-memory approximation. Thus, only very recent information is relevant to the present behavior. This approximation simplifies Eq. (5) to the classical diffusion equation, where $D(x,t)$ reduces to a constant and is identified as the diffusion coefficient. Equation (5) is an approximation of the full quantum description where short-time correlations contribute to the coefficient $D(x,t)$.

The steady states observed in our simulations suggest that the systems may be described by kinetic equations [53,54,67,68], where an effective description of the density rather than the wave function can be applied. By analyzing the evolution of density profiles following a suddenly induced interaction imbalance, we identify a constant density gradient across the interface of the interaction imbalance when the steady-state current lasts, as illustrated in the shaded regions in Figs. 9(a) and 9(b) for the BHM and FHM and in the inset in Fig. 7(b) for the continuum model.

Fick’s law relates the mass current and density gradient and implies diffusion-like behavior. Assuming that the isolated systems in the quasi–steady states follow the kinetic equations, we can estimate the diffusion coefficient defined by

$$D_{B(F)} = \frac{\overline{J_{B(F)}}}{\nabla_i n_i^{B(F)}}. \quad (6)$$

The averages are taken in the same time window, the spatial gradient is taken along the lattice, and only the steady-state density gradient at the interaction-imbalance interface is considered. In Figs. 9(c) and 9(d), we show the diffusion coefficients extracted from the BHM and FHM following a

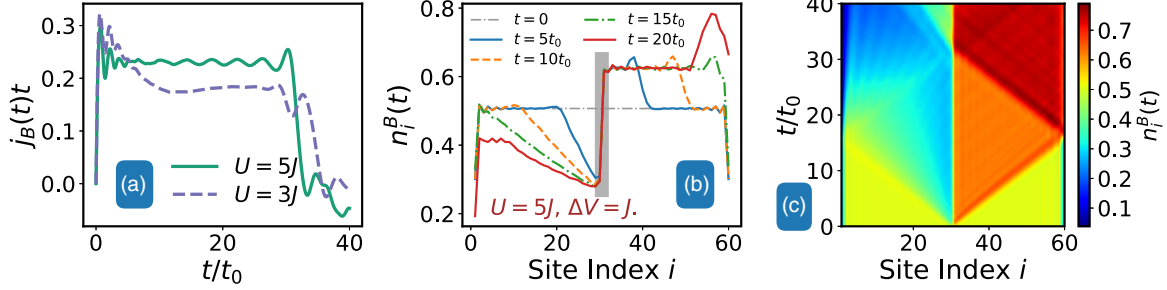


FIG. 10. QSSC in potential-induced transport in the BHM with $\bar{n}_B = 1/2$. The on-site potential energy in the left half of the system experiences a sudden change of $\Delta V = J$. (a) Current versus time for two systems with different initial interactions $U = 3J$ (dashed line) and $U = 5J$ (solid line). (b) Density profiles at different times and (c) density contour for a system with initial interaction $U = 5J$.

sudden quench of interaction imbalance. Importantly, due to memory effects of initial states, the diffusion coefficients are sensitive to the initial conditions even if the final Hamiltonians are the same. Therefore, in isolated interacting systems the diffusion coefficients can inherit the long-time memory of initial states.

The diffusion coefficient exhibits an interesting dependence on the spin statistics. With a fixed initial interaction, the diffusion coefficient increases with interaction imbalance in both spin statistics, although the variation in the BHM is very limited. On the other hand, with a fixed interaction imbalance, the diffusion coefficient of the BHM (FHM) increases (decreases) monotonically as the initial interaction increases. Our results, however, do not exclude the possibilities that the transport behavior is more complicated than the kinetic equations or their generalizations.

We remark that Eq. (6) may be more common than previously thought. For instance, the spreading of a single-particle Gaussian wave packet has both time and initial state dependence. The wave function of a single-particle Gaussian wave is the packet [79]

$$\psi(x, t) = \left[\frac{1}{\sigma[1 + i(t/\tau)]\sqrt{2\pi}} \right]^{\frac{1}{2}} \exp \left\{ -\frac{1}{4} \frac{(x-a)^2}{\sigma^2[1 + i(t/\tau)]} \right\}. \quad (7)$$

The initial condition has a normal distribution with mean $\langle x \rangle = a$ and variance $\langle (x-a)^2 \rangle = \sigma^2$, and we define $\tau = 2m\sigma^2/\hbar^2$. The probability distribution is $P(x, t) = |\psi(x, t)|^2 = \frac{1}{\sigma(t)\sqrt{2\pi}} \exp \left\{ -\frac{1}{2} \left[\frac{x-a}{\sigma(t)} \right]^2 \right\}$, where $\sigma(t) = \sigma\sqrt{1 + (t/\tau)^2}$. This wave packet has a fixed mean ($x = a, \forall t$) but a growing variance. The current density can be obtained from Eq. (7) as

$$j = \frac{\hbar}{2mi} [\psi^* \nabla \psi - (\nabla \psi^*) \psi] = -\frac{\hbar(t/\tau)}{2m} \nabla P(x, t). \quad (8)$$

By using $\nabla P(x, t) = -\frac{x-a}{\sigma^2(t)} P(x, t)$ and comparing the result with Eq. (5), we conclude that

$$D(t) = \frac{\hbar^3}{4m^2\sigma^2} t. \quad (9)$$

The diffusion coefficient obtained here is a time-dependent function instead of a constant.

VI. MEMORY EFFECTS IN POTENTIAL-INDUCED TRANSPORT

Alternatively, one can use a potential imbalance to drive a current while keeping the interaction uniform. The time-dependent part of the Hamiltonian is an on-site potential,

$$H_{\text{BHM}}(t) = \mathcal{H}_{\text{BHM}} + \sum_i V(i, t) n_i, \quad (10)$$

for the BHM and

$$H_{\text{FHM}}(t) = \mathcal{H}_{\text{FHM}} + \sum_{i,\sigma} V(i, t) n_{i,\sigma} \quad (11)$$

for the FHM. \mathcal{H}_{BHM} and \mathcal{H}_{FHM} are defined in Eqs. (1) and (2) with $U(i, t) = U, \forall i, t$. Initially, the potential energy is uniform, $V(i, t \leq 0) = 0, \forall i$, and the system is in the ground state. A current can be induced by introducing a step-function imbalance in the potential energy so that $V(i \in L, t \geq 0) = \Delta V = J$ as shown in Fig. 10. The QSSC emerges again in potential-induced transport, so we are able to identify the memory effects in this settings. We mention that the potential bias is applied uniformly to the left half of the system, unlike the constant potential gradient across the entire system as implemented in the study of Bloch oscillations [80,81].

A downside of potential-induced transport is that in isolated systems, energy conservation prevents exchange of particles if the potential imbalance is larger than the bandwidth [32]. As a consequence, the system enters a dynamically insulating state if $\Delta V > 4J$. Therefore, here we only demonstrate two values of potential imbalance, $\Delta V = J$ and $2J$.

From the values of QSSCs we can determine whether there are memory effects of initial states or switching protocols in potential-induced transport. The results are summarized in Fig. 11. The QSSCs clearly depend on the initial interaction U , and when U/J is small the QSSC increases with the uniform interaction. By comparing two QSSCs with two different interactions but with the same ΔV in Fig. 11(b), the memory effects of initial states are clearly identified. In contrast, Figs. 11(c) and 11(d) show that two systems with the same initial uniform interaction U and potential imbalance ΔV but with different ramping times have the same steady-state QSSC values. In the available parameter space, we found that memory effects of switching protocols are not resolvable in potential-induced transport in lattices, mainly due to the limited potential difference, which should be less than the

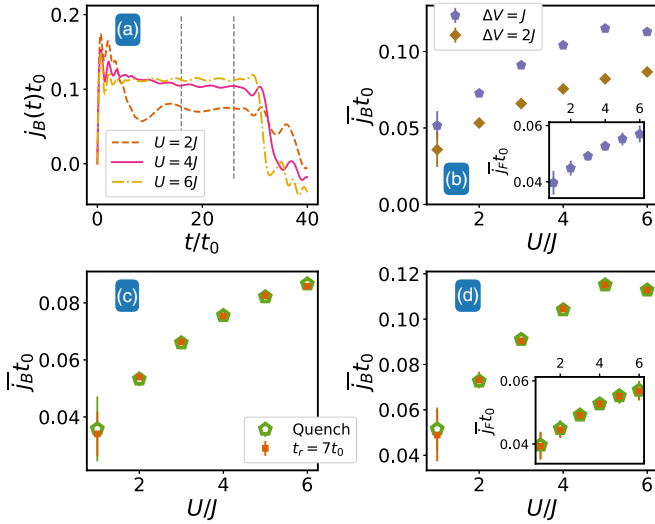


FIG. 11. Currents in potential-induced transport of the BHM with $L=60$ sites and $\bar{n}_B=1/2$. (a) Currents at the interface of the potential imbalance versus time for different uniform b interactions. Here $\Delta V=J$. (b) QSSCs from systems with different uniform interactions, showing a clear dependence on the initial states. Insets: Results for the FHM with $\bar{n}_F=1/6$ and similar parameters. (c, d) Averaged steady-state values from different ramping times when the same potential imbalance is switched on linearly in time. $\Delta V=2J$ in (c) and $\Delta V=J$ in (d), and all symbols overlap within the error bars for each U . Memory effects of switching protocols are not resolvable here.

bandwidth. The same conclusions can be drawn for the FHM and the results are shown in the insets in Figs. 11(b) and 11(d).

VII. EXPERIMENTAL IMPLICATIONS

The mass current can be experimentally obtained from the time derivative of the density profile [82–86]. In order to observe quasi-steady states, one may need at least 30 lattice sites [87,88]. The memory effects of initial states can be maximized by using two systems with very different initial interactions so their initial ground states are distinct. For the memory effects of switching protocols, one has to ramp the interaction imbalance with different time scales, and our results suggest that fermions at half-filling or bosons at unity filling will exhibit stronger memory effects. However, the stronger interaction energy limits the time window for measuring the QSSC and this limitation is also discussed. The memory effects presented here should survive in the thermodynamic limit when the system size becomes infinity as long as no additional relaxation is introduced. Since the BHM supports superfluids, dissipation effects such as phase slip [89,90] may relax the system and eventually wash out the memory effects found here.

Both fermionic and bosonic quantum atomic gases can be trapped in 1D lattices [91–94], and the interactions between atoms can be tuned by external magnetic fields or optical means [95]. A spatial interaction imbalance can be produced experimentally by a nonuniform magnetic field [95,96], or optical control of atomic collisions [97–103]. Reference [97] has demonstrated a spatial density modulation using an optical Feshbach resonance of bosons, and one may also use inhomogeneous confinement potentials to modulate the

interactions in real space [104–107]. The external magnetic field can change the initial interaction [95], while the optical control provides an interaction imbalance. Although it may be possible to use a nonuniform magnetic field to induce interaction imbalance, the challenge is to make the interface separating regions with different interactions narrow compared to the atomic cloud size. By making the spatially imbalanced interaction time dependent, one can drive the system out of equilibrium and probe memory effects. We remark that allowing a finite width of the interaction-imbalance interface does not lead to any qualitative difference in our findings if the width is small, but as the temperature increases, the smooth spreading of the particle distribution is expected to reduce quantum memory effects.

VIII. CONCLUSION

Interaction-induced transport properties are shown to be a versatile platform for studying quantum dynamics, in particular, steady-state memory effects. For dilute atomic gases, the value of a QSSC increases (decreases) as a stronger interaction imbalance (initial interaction) is applied to an isolated system. For bosons with unity filling and fermions with half-filling, the behavior is qualitatively the same, and breakdown of the Mott insulating state has been found with both statistics. In contrast to electronic systems, where external relaxation mechanisms such as interactions with impurities and the background ionic lattice bring the systems into a unique equilibrium or steady state, in isolated quantum systems without relaxation long-time memory effects can persist. Evidence of memory effects in the quasi-steady states induced by interaction imbalance has been presented here for both the BHM and the FHM. Memory effects of the initial states are quite prevalent, but memory effects of the switching protocols are mostly visible only in lattice interaction-induced transport. The memory effects discussed here in isolated quantum systems can be understood in the following way: As the states evolve with different but conserved energies, they result in different final steady states even if the final Hamiltonian is the same. Similar effects are also discussed in doublon dynamics in both theoretical and experimental studies [108–111], where the highly occupied states cannot be easily relaxed due to energy conservation.

Memory effects of steady-state currents in isolated quantum systems can lead to nonconstant diffusion coefficients if the kinetic-equation approach is used to describe the steady-state behavior. Moreover, the steady-state current in quantum systems may find future applications. For instance, atomic superfluids in a ring-shaped potential may simulate superconducting devices [112]. Exploiting memory effects of steady-state currents in isolated systems may lead to alternative designs of quantum devices as proposed in Ref. [35].

ACKNOWLEDGMENTS

We thank Massimiliano Di Ventra and Micheal Zwolak for stimulating discussions. The tDMRG programs are built upon the universal tensor library (Uni10) [113]. Some of the simulations were carried out by the Merced Cluster at UC Merced, supported by the National Science Foundation (Grant No. ACI-1429783).

- [1] R. W. Schoenlein, W. Z. Lin, J. G. Fujimoto, and G. L. Eesley, *Phys. Rev. Lett.* **58**, 1680 (1987).
- [2] T. W. Roberti, B. A. Smith, and J. Z. Zhang, *J. Chem. Phys.* **102**, 3860 (1995).
- [3] J. Y. Bigot, J. C. Merle, O. Cregut, and A. Daunois, *Phys. Rev. Lett.* **75**, 4702 (1995).
- [4] G. Bertotti, *Hysteresis in Magnetism: For Physicists, Materials Scientists, and Engineers*, Academic Press Series in Electromagnetism (Academic Press, New York, 1998).
- [5] E. Jagla, *Papers Phys.* **9**, 090004 (2017).
- [6] Y. V. Pershin and M. Di Ventra, *Adv. Phys.* **60**, 145 (2011).
- [7] R. Marani, G. Gelao, and A. G. Perri, *Int. J. Adv. Eng. Technol.* **8**, 294 (2015).
- [8] I. Gilbert, G.-W. Chern, B. Fore, Y. Lao, S. Zhang, C. Nisoli, and P. Schiffer, *Phys. Rev. B* **92**, 104417 (2015).
- [9] X. Zhao, M. A. McLain, J. Vijande, A. Ferrando, L. D. Carr, and M. Á. García-March, [arXiv:1705.02051](https://arxiv.org/abs/1705.02051).
- [10] C. L. Folcia, M. J. Tello, and J. M. Pérez-Mato, *Phys. Rev. B* **36**, 7181 (1987).
- [11] V. P. Aliyev, S. S. Babayev, T. G. Mammadov, M.-H. Y. Seyidov, and R. A. Suleymanov, *Solid State Commun.* **128**, 25 (2003).
- [12] X. Marti, I. Fina, C. Frontera, J. Liu, P. Wadley, Q. He, R. J. Paull, J. D. Clarkson, J. Kudrnovský, I. Turek *et al.*, *Nat. Mater.* **13**, 367 (2014).
- [13] Y. Sun, M. B. Salamon, K. Garnier, and R. S. Averback, *Phys. Rev. Lett.* **91**, 167206 (2003).
- [14] J. Maldacena, S. H. Shenker, and D. Stanford, *J. High Energy Phys.* **08** (2016) 106.
- [15] A. Polkovnikov, K. Sengupta, A. Silva, and M. Vengalattore, *Rev. Mod. Phys.* **83**, 863 (2011).
- [16] M. Pasienski, D. McKay, M. White, and B. DeMarco, *Nat. Phys.* **6**, 677 (2010).
- [17] C. Meldgin, U. Ray, P. Russ, D. Chen, D. M. Ceperley, and B. DeMarco, *Nat. Phys.* **12**, 646 (2016).
- [18] S. S. Kondov, W. R. McGehee, W. Xu, and B. DeMarco, *Phys. Rev. Lett.* **114**, 083002 (2015).
- [19] M. H. Fischer, M. Maksymenko, and E. Altman, *Phys. Rev. Lett.* **116**, 160401 (2016).
- [20] M. Schreiber, S. S. Hodgman, P. Bordia, H. P. Lüschen, M. H. Fischer, R. Vosk, E. Altman, U. Schneider, and I. Bloch, *Science* **349**, 842 (2015).
- [21] J. Smith, A. Lee, P. Richerme, B. Neyenhuis, P. W. Hess, P. Hauke, M. Heyl, D. A. Huse, and C. Monroe, *Nat. Phys.* **12**, 907 (2016).
- [22] N. Tsuji, P. Werner, and M. Ueda, *Phys. Rev. A* **95**, 011601 (2017).
- [23] B. Dóra and R. Moessner, *Phys. Rev. Lett.* **119**, 026802 (2017).
- [24] F. M. Haehl, R. Loganayagam, P. Narayan, and M. Rangamani, [arXiv:1701.02820](https://arxiv.org/abs/1701.02820).
- [25] N. Y. Yao, F. Grusdt, B. Swingle, M. D. Lukin, D. M. Stamper-Kurn, J. E. Moore, and E. A. Demler, [arXiv:1607.01801](https://arxiv.org/abs/1607.01801).
- [26] C.-C. Chien, S. Peotta, and M. Di Ventra, *Nat. Phys.* **11**, 998 (2015).
- [27] S. Eckel, J. G. Lee, F. Jendrzejewski, N. Murray, C. W. Clark, C. J. Lobb, W. D. Phillips, M. Edwards, and G. K. Campbell, *Nature (London)* **506**, 200 (2014).
- [28] M. Metcalf, C.-Y. Lai, and C.-C. Chien, *Phys. Rev. A* **93**, 053617 (2016).
- [29] J. I. Costa-Filho, R. B. B. Lima, R. R. Paiva, P. M. Soares, W. A. M. Morgado, R. L. Franco, and D. O. Soares-Pinto, *Phys. Rev. A* **95**, 052126 (2017).
- [30] Z.-X. Man, Y.-J. Xia, and R. Lo Franco, *Phys. Rev. A* **92**, 012315 (2015).
- [31] H. D. Cornean, A. Jensen, and G. Nenciu, *Ann. Henri Poincaré* **15**, 1919 (2014).
- [32] C.-C. Chien, D. Gruss, M. Di Ventra, and M. Zwolak, *New J. Phys.* **15**, 063026 (2013).
- [33] C.-C. Chien and M. Di Ventra, *Phys. Rev. A* **87**, 023609 (2013).
- [34] C.-C. Chien, M. Di Ventra, and M. Zwolak, *Phys. Rev. A* **90**, 023624 (2014).
- [35] C.-Y. Lai and C.-C. Chien, *Phys. Rev. Appl.* **5**, 034001 (2016).
- [36] Y. He and C.-C. Chien, *Phys. Rev. B* **94**, 024308 (2016).
- [37] M. Metcalf, C.-Y. Lai, K. Wright, and C.-C. Chien, *Europhys. Lett.* **118**, 56004 (2017).
- [38] D. Wang, S. Xu, Y. Wang, and C. Wu, *Phys. Rev. B* **91**, 115118 (2015).
- [39] M.-C. Chung, Y.-H. Jhu, P. Chen, and C.-Y. Mou, *J. Phys.: Condens. Matter* **25**, 285601 (2013).
- [40] M. Rigol, A. Muramatsu, and M. Olshanii, *Phys. Rev. A* **74**, 053616 (2006).
- [41] M. Rigol, V. Dunjko, V. Yurovsky, and M. Olshanii, *Phys. Rev. Lett.* **98**, 050405 (2007).
- [42] M.-C. Chung, A. Iucci, and M. A. Cazalilla, *New J. Phys.* **14**, 075013 (2012).
- [43] E. Perfetto, G. Stefanucci, and M. Cini, *Phys. Rev. Lett.* **105**, 156802 (2010).
- [44] S. R. White, *Phys. Rev. Lett.* **69**, 2863 (1992).
- [45] S. R. White, *Phys. Rev. B* **48**, 10345 (1993).
- [46] S. Östlund and S. Rommer, *Phys. Rev. Lett.* **75**, 3537 (1995).
- [47] U. Schollwöck, *Rev. Mod. Phys.* **77**, 259 (2005).
- [48] I. P. McCulloch, *J. Stat. Mech.* (2007) P10014.
- [49] U. Schollwöck, *Ann. Phys.* **326**, 96 (2011).
- [50] S. R. White and A. E. Feiguin, *Phys. Rev. Lett.* **93**, 076401 (2004).
- [51] C.-Y. Lai, J.-T. Hung, C.-Y. Mou, and P. Chen, *Phys. Rev. B* **77**, 205419 (2008).
- [52] G. Vidal, *Phys. Rev. Lett.* **93**, 040502 (2004).
- [53] A. Kamenev, *Field Theory of Non-Equilibrium Systems* (Cambridge University Press, Cambridge, UK, 2011).
- [54] M. Di Ventra, *Electrical Transport in Nanoscale Systems* (Cambridge University Press, Cambridge, UK, 2010).
- [55] C.-C. Chien and M. Di Ventra, *Europhys. Lett.* **99**, 40003 (2012).
- [56] M. Di Ventra and T. N. Todorov, *J. Phys.: Condens. Matter* **16**, 8025 (2004).
- [57] R. Labouvie, B. Santra, S. Heun, S. Wimberger, and H. Ott, *Phys. Rev. Lett.* **115**, 050601 (2015).
- [58] C.-Y. Lai and C.-C. Chien, *Sci. Rep.* **6**, 37256 (2016).
- [59] T. Oka, R. Arita, and H. Aoki, *Phys. Rev. Lett.* **91**, 066406 (2003).
- [60] T. Oka and H. Aoki, *Phys. Rev. Lett.* **95**, 137601 (2005).
- [61] F. Heidrich-Meisner, I. González, K. A. Al-Hassanieh, A. E. Feiguin, M. J. Rozenberg, and E. Dagotto, *Phys. Rev. B* **82**, 205110 (2010).
- [62] T. D. Kühner, S. R. White, and H. Monien, *Phys. Rev. B* **61**, 12474 (2000).
- [63] J. Zakrzewski and D. Delande, *AIP Conf. Proc.* **1076**, 292 (2008).

- [64] E. M. Conwell, *Phys. Today* **23**(6), 35 (2008).
- [65] T. Oka and H. Aoki, *Phys. Rev. B* **81**, 033103 (2010).
- [66] E. H. Lieb and F. Y. Wu, *Physica A* **321**, 1 (2003).
- [67] W. T. Grandy, Jr., *Entropy and the Time Evolution of Macroscopic Systems*, International Series of Monographs on Physics (Oxford University Press, Oxford, UK, 2008).
- [68] A. Altland and B. D. Simons, *Condensed Matter Field Theory*, Cambridge Books Online (Cambridge University Press, Cambridge, NY, 2010).
- [69] E. P. Gross, *Nuovo Cimento* **20**, 454 (1961).
- [70] L. P. Pitaevskii, *Zh. Eksp. Teor. Fiz.* **40**, 646 (1961) [*JETP* **13**, 451 (1961)].
- [71] D. Vudragović, I. Vidanović, A. Balaž, P. Muruganandam, and S. K. Adhikari, *Comput. Phys. Commun.* **183**, 2021 (2012).
- [72] C. J. Pethick and H. Smith, *Bose–Einstein Condensation in Dilute Gases*, 2nd ed. (Cambridge University Press, Cambridge, UK, 2010).
- [73] H. T. C. Stoof, D. B. M. Dickerscheid, and K. Gubbels, *Ultracold Quantum Fields. Theoretical and Mathematical Physics* (Springer Netherlands, Dordrecht, 2008).
- [74] M. Rab, J. H. Cole, N. G. Parker, A. D. Greentree, L. C. L. Hollenberg, and A. M. Martin, *Phys. Rev. A* **77**, 061602 (2008).
- [75] C. J. Bradley, M. Rab, A. D. Greentree, and A. M. Martin, *Phys. Rev. A* **85**, 053609 (2012).
- [76] P. Muruganandam and S. K. Adhikari, *Comput. Phys. Commun.* **180**, 1888 (2009).
- [77] M. M. Cerimele, M. L. Chiofalo, F. Pistella, S. Succi, and M. P. Tosi, *Phys. Rev. E* **62**, 1382 (2000).
- [78] R. Landauer, *IBM J. Res. Dev.* **1**, 223 (1957).
- [79] J. J. Sakurai and J. Napolitano, *Modern Quantum Mechanics* (Addison-Wesley, Reading, MA, 2011).
- [80] T. Dekorsy, R. Ott, H. Kurz, and K. Köhler, *Phys. Rev. B* **51**, 17275 (1995).
- [81] H. Flayac, D. D. Solnyshkov, and G. Malpuech, *Phys. Rev. B* **83**, 045412 (2011).
- [82] D. Greif, M. F. Parsons, A. Mazurenko, and C. S. Chiu, *Science* **351**, 953 (2016).
- [83] M. F. Parsons, A. Mazurenko, C. S. Chiu, G. Ji, D. Greif, and M. Greiner, *Science* **353**, 1253 (2016).
- [84] L. W. Cheuk, M. A. Nichols, K. R. Lawrence, M. Okan, H. Zhang, and M. W. Zwierlein, *Phys. Rev. Lett.* **116**, 235301 (2016).
- [85] M. Leder, C. Grossert, L. Sitta, M. Genske, A. Rosch, and M. Weitz, *Nat. Commun.* **7**, 13112 (2016).
- [86] M. Miranda, R. Inoue, Y. Okuyama, A. Nakamoto, and M. Kozuma, *Phys. Rev. A* **91**, 063414 (2015).
- [87] C.-C. Chien, M. Zwolak, and M. Di Ventra, *Phys. Rev. A* **85**, 041601 (2012).
- [88] N. Bushong, N. Sai, and M. Di Ventra, *Nano Lett.* **5**, 2569 (2005).
- [89] D. McKay, M. White, M. Pasienski, and B. De Marco, *Nature (London)* **453**, 76 (2008).
- [90] S. S. Abbate, L. Gori, M. Inguscio, G. Modugno, and C. D’Errico, *Eur. Phys. J. Spec. Topics* **226**, 2815 (2017).
- [91] D. Jaksch and P. Zoller, *Ann. Phys.* **315**, 52 (2005).
- [92] I. Bloch, J. Dalibard, and W. Zwerger, *Rev. Mod. Phys.* **80**, 885 (2008).
- [93] O. Morsch, M. Cristiani, J. H. Müller, D. Ciampini, and E. Arimondo, *Phys. Rev. A* **66**, 021601 (2002).
- [94] T. Esslinger, *Annu. Rev. Condens. Matter Phys.* **1**, 129 (2010).
- [95] C. Chin, R. Grimm, P. S. Julienne, and E. Tiesinga, *Rev. Mod. Phys.* **82**, 1225 (2010).
- [96] C. H. Schunck, M. W. Zwierlein, C. A. Stan, S. M. F. Raupach, W. Ketterle, A. Simoni, E. Tiesinga, C. J. Williams, and P. S. Julienne, *Phys. Rev. A* **71**, 045601 (2005).
- [97] L. W. Clark, L. C. Ha, C. Y. Xu, and C. Chin, *Phys. Rev. Lett.* **115**, 155301 (2015).
- [98] Z. Fu, P. Wang, L. Huang, Z. Meng, H. Hu, and J. Zhang, *Phys. Rev. A* **88**, 041601 (2013).
- [99] R. Yamazaki, S. Taie, S. Sugawa, and Y. Takahashi, *Phys. Rev. Lett.* **105**, 050405 (2010).
- [100] F. K. Fatemi, K. M. Jones, and P. D. Lett, *Phys. Rev. Lett.* **85**, 4462 (2000).
- [101] K. Enomoto, K. Kasa, M. Kitagawa, and Y. Takahashi, *Phys. Rev. Lett.* **101**, 203201 (2008).
- [102] T. Fukuhara, S. Sugawa, Y. Takasu, and Y. Takahashi, *Phys. Rev. A* **79**, 021601 (2009).
- [103] H. Wu and J. E. Thomas, *Phys. Rev. Lett.* **108**, 010401 (2012).
- [104] R. Stock and I. H. Deutsch, *Phys. Rev. A* **73**, 032701 (2006).
- [105] H. Moritz, T. Stöferle, K. Günter, M. Köhl, and T. Esslinger, *Phys. Rev. Lett.* **94**, 210401 (2005).
- [106] G. A. Sekh, *Phys. Lett. A* **376**, 1740 (2012).
- [107] E. Tiesinga, C. J. Williams, F. H. Mies, and P. S. Julienne, *Phys. Rev. A* **61**, 063416 (2000).
- [108] S. D. Huber and A. Rüegg, *Phys. Rev. Lett.* **102**, 065301 (2009).
- [109] N. Strohmaier, D. Greif, R. Jördens, L. Tarruell, H. Moritz, T. Esslinger, R. Sensarma, D. Pekker, E. Altman, and E. Demler, *Phys. Rev. Lett.* **104**, 080401 (2010).
- [110] J. P. Covey, S. A. Moses, M. Gärtner, A. Safavi-Naini, M. T. Miecnikowski, Z. Fu, J. Schachenmayer, P. S. Julienne, A. M. Rey, D. S. Jin *et al.*, *Nat. Commun.* **7**, 11279 (2016).
- [111] R. Rausch and M. Potthoff, *Phys. Rev. B* **95**, 045152 (2017).
- [112] C. Ryu, P. W. Blackburn, A. A. Blinova, and M. G. Boshier, *Phys. Rev. Lett.* **111**, 205301 (2013).
- [113] Y. J. Kao, Y. D. Hsieh, and P. Chen, *J. Phys.: Conf. Ser.* **640**, 012040 (2015).